JOURNAL OF MODERN OPTICS, 1994, VOL. 41, NO. 8, 1637–1652

Contouring by electronic speckle pattern interferometry employing divergent dual beam illumination

Y. ZOU, G. PEDRINI and H. TIZIANI
University of Stuttgart, Institute of Applied Optics,
Pfaffenwaldring 9, 70569 Stuttgart, Germany

(*Received 10 December 1993; revision received 4 March 1994*)

Abstract. For contouring of large object surfaces by means of electronic speckle pattern interferometry divergent illuminations were used. A method to shift dual illumination beams was employed to obtain contour fringes. The relationship between the fringes and object depth does not have the same form as in the case of collimated illuminations. It shows that the original measurement data can be corrected. Theoretical analysis and experimental results are presented which are in agreement with each other.

1. Introduction

A currently developed double-pulse electronic speckle interferometry technique is well suited for studying vibrations, especially transient ones [1–2]. For three-dimensional vibration analysis the shape of the object should be known. The information about the object shape can be obtained through either a Moiré, a fringe pattern projection, a holographic interferometry or an electronic speckle pattern interferometry (ESPI) method. It is relatively simple to measure the deformation or vibration and the shape of an object by using one ESPI system. Moreover, the sensitivity in an ESPI contouring system can be easily controlled and continuously changed. The sensitivity vector in our system is situated along the view direction, which provides simple fringe interpolation.

For large surface topography divergent illumination is useful. It minimizes the size, the complexity and also the cost of equipment for the measurements. It is also flexible enough to measure objects with different sizes. In existing dual-beam ESPI contouring methods, either a collimated [3–5] or a divergent beam [6–7] is used for illuminating the test object. The contour interval in a dual-beam ESPI arrangement with collimated illumination is $d=\lambda/(2\delta\theta\sin\theta)$, where λ is the wavelength of the illumination, θ is the illumination angle and $\delta\theta$ is the angle change of the object tilting [8] or of the beam [9] between two exposures. However, when divergent illumination is used, this relation is no longer valid.

A theoretical analysis of ESPI contouring with divergent dual-beam illumination is given in this paper. The measured phase data are not only object depth dependent but also object dimension dependent. To obtain the correct information on the object depth a numerical method should ideally be introduced to solve the complex formula. But in most cases the measured phase can either be experimentally or analytically corrected with some approximations. These approximations were employed in our experiments and will be discussed in detail in this paper. In the chosen experimental configuration the illumination beams were shifted; however, the analysis would also apply if the object was tilted.

2. Theoretical layout

The basic principle of ESPI can be found, for example, in [10, 11]. Two intensity patterns of speckle images at two states of the object are recorded using television or charge coupled device (CCD) camera techniques. The correlation between these two states can be mapped by correlation fringes from electronic or digital subtraction or addition of the two intensity patterns. The phase difference between these states is manifested in the fringes. The principle can be applied for deformation or vibration analysis as well as for contouring. When this phase difference is related to the depth of the object, the shape of the object can be obtained from the fringe pattern. In the following we give a geometrical analysis of the relationship between the phase difference and the depth of the object leading to contouring, by dual-beam ESPI based on shifting divergent illumination beams.

The object is illuminated by two spherical waves from either side symmetrically about the view direction Z, as shown in figure 1. O is the origin of the coordinate system, M is an arbitrary point on the test surface, and N is a reference point which is located on the axis Z close to the object surface; $\mathbf{r}$ is the position vector from point N to M and can be written as $\mathbf{r}=(x, y, z-z_n)$. P is the viewpoint which is located on the Z axis; $\mathbf{a}$ is the position vector from point P to M. $\mathbf{K}_1$ and $\mathbf{K}_2$ are the unit direction vectors of the waves from sources S_1 and S_2 to M, respectively; l_1 and l_2 are the path lengths from the sources to point M and l_0 is the path length from one source to point N. The coordinates of each point are $S_1(x_s,0,0)$, $S_2(-x_s,0,0)$, $N(0,0,z_n)$, $M(x,y,z)$, $P(0,0,z_p)$ and O(0,0,0). The phases associated with the optical paths from the sources to the viewpoint P passing point M, ϕ_1 and ϕ_2, are given by

$$\phi_1=\frac{2\pi}{\lambda}(l_1+|\mathbf{a}|),$$

$$\phi_2=\frac{2\pi}{\lambda}(l_2+|\mathbf{a}|), \tag{1}$$

where λ is the wavelength of illumination and $|\mathbf{a}|$ is the scalar magnitude of $\mathbf{a}$. They can also be represented as multiplication of vectors:

$$\phi_1=\frac{2\pi}{\lambda}[(\mathbf{l}_{01}+\mathbf{r})\cdot\mathbf{K}_1+|\mathbf{a}|],$$

$$\phi_2=\frac{2\pi}{\lambda}[(\mathbf{l}_{02}+\mathbf{r})\cdot\mathbf{K}_2+|\mathbf{a}|], \tag{2}$$

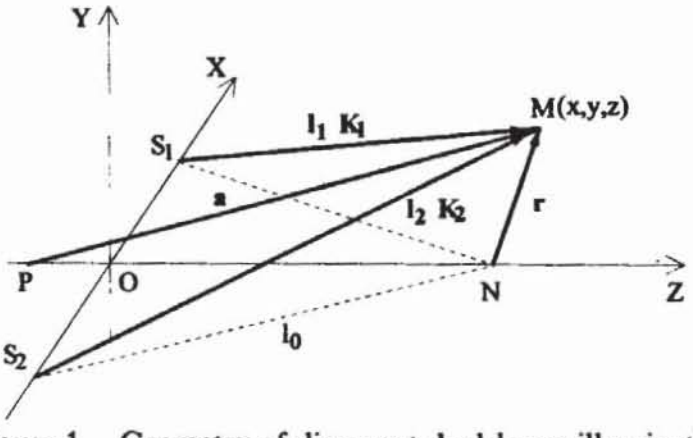

Figure 1. Geometry of divergent dual-beam illumination.

where $\mathbf{l}_{01}$ and $\mathbf{l}_{02}$ are the vectors from sources S_1 and S_2 to the reference point N, respectively; they have the same magnitude l_0 (see figure 2). The phase of the interference between these two rays then has the form

$$\Phi=\phi_1-\phi_2=\frac{2\pi}{\lambda}[\mathbf{l}_{01}\cdot\mathbf{K}_1-\mathbf{l}_{02}\cdot\mathbf{K}_2+\mathbf{r}\cdot(\mathbf{K}_1-\mathbf{K}_2)]. \tag{3}$$

After the beams (or, in other words, the sources) are shifted, the phase is changed to

$$\Phi'=\frac{2\pi}{\lambda}[\mathbf{l}'_{01}\cdot\mathbf{K}'_1-\mathbf{l}'_{02}\cdot\mathbf{K}'_2+\mathbf{r}\cdot(\mathbf{K}'_1-\mathbf{K}'_2)]. \tag{4}$$

The phase difference between these two conditions is then

$$\begin{aligned}\Delta\Phi&=\Phi'-\Phi\\&=\frac{2\pi}{\lambda}[C(\alpha_1,\alpha_2,\theta_1,\theta_2)+\mathbf{r}\cdot(\Delta\mathbf{K}_1-\Delta\mathbf{K}_2)],\end{aligned} \tag{5}$$

where $\Delta\mathbf{K}_1=(\mathbf{K}'_1-\mathbf{K}_1)$, $\Delta\mathbf{K}_2=(\mathbf{K}'_2-\mathbf{K}_2)$, and $C(\alpha_1,\alpha_2,\theta_1,\theta_2)=(\mathbf{l}'_{01}\cdot\mathbf{K}'_1-\mathbf{l}'_{02}\cdot\mathbf{K}'_2-\mathbf{l}_{01}\cdot\mathbf{K}_1+\mathbf{l}_{02}\cdot\mathbf{K}_2)$ which is an angle-dependent parameter (see Appendix A). α_1 is the angle between $\mathbf{K}_1$ and the X–Z plane; α_2 is the angle between $\mathbf{K}_2$ and the X–Z plane. θ_1 is the angle between the projection of $\mathbf{K}_1$ on the X–Z plane and Z axis; θ_2 is the angle between the projection of $\mathbf{K}_2$ on the X–Z plane and Z axis. In practice, sources S_1 and S_2 are two reflected images of one point source. When this point source is shifted by $\Delta\mathbf{S}$, S_1 or S_2 introduces a shift of $\Delta\mathbf{S}_1$ or $\Delta\mathbf{S}_2$, respectively, and $|\Delta\mathbf{S}_1|=|\Delta\mathbf{S}_2|=|\Delta\mathbf{S}|$. The schematic geometry of dual-beam shifted contouring is partially shown in figure 2 (all parameters corresponding to source S_1. θ_0 is the angle between $\mathbf{l}_{01}$ or $\mathbf{l}_{02}$ and the Z axis. In principle all parameters of $\alpha_1, \alpha_2, \theta_1, \theta_2, \Delta\mathbf{K}_1$ and $\Delta\mathbf{K}_2$ in equation (5) are functions of the location of point M on the object. The measured phase $\Delta\Phi$ is not simply related to $\mathbf{r}$. To obtain an accurate result a numerical solution to equation (5) should be taken. But in practical experiments we can easily set some conditions to simplify the parameter relations in this equation.

Normally the shift of the source is some hundred micrometres, which is much smaller than the dimension of the optical set-up. When the source is shifted in the X–

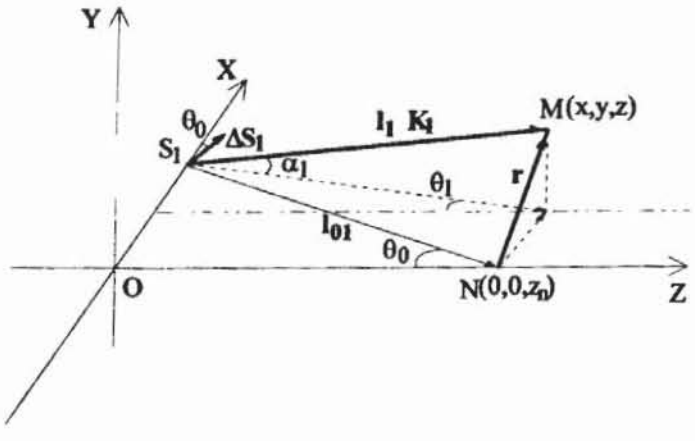

Figure 2. Geometry of dual-beam shifted contouring.

Z plane and the direction of the shift is perpendicular to the principal ray of the illumination, we obtain (see Appendices A and B):

$$\begin{aligned}\Delta\Phi = &-\frac{2\pi\Delta S}{\lambda}\Big\{\cos\alpha_1\sin(\theta_1+\theta_0)+\cos\alpha_2\sin(\theta_2+\theta_0)\\&+\frac{x_s}{z}(\cos\alpha_1\cos^2\theta_1+\cos\alpha_2\cos^2\theta_2)\\&+\frac{z_n}{2z}[\sin(2\theta_1)\cos\alpha_1+\sin(2\theta_2)\cos\alpha_2]\Big\}\\&+\frac{2\pi\Delta S}{\lambda}\Big\{\frac{x}{z}(\cos\alpha_1\cos^2\theta_1-\cos\alpha_2\cos^2\theta_2)\\&+y\cos\theta_0\left(\frac{\sin\alpha_1\cos\alpha_1}{((x-x_s)^2+z^2)^{1/2}}-\frac{\sin\alpha_2\cos\alpha_2}{((x+x_s)^2+z^2)^{1/2}}\right)\\&-\frac{z-z_n}{2z}[\cos\alpha_1\sin(2\theta_1)+\cos\alpha_2\sin(2\theta_2)]\Big\}\\=&\Delta\Phi(x,y,z),\end{aligned}\tag{6}$$

where $\alpha_1=\alpha_1(x,y,z)$, $\alpha_2=\alpha_2(x,y,z)$, $\theta_1=\theta_1(x,z)$ and $\theta_2=\theta_2(x,z)$. This equation can still only be evaluated numerically. If the dimension of the measuring object is much smaller than the distance between the source and the object (i.e. $z_n\gg|\mathbf{r}|$ or $z_n\gg|x|$, $|y|$, $|z-z_n|$, to allow $\cos\alpha_1\cong\cos\alpha_2\cong1$, $\sin\alpha_1\cong\sin\alpha_2\cong0$, $\theta_1\cong\arctan[(x_s-x)/z_n]$ and $\theta_2\cong\arctan[(x_s+x)/z_n]$, equation (6) approximates to (Appendices A and B):

$$\begin{aligned}\Phi\cong&-\frac{2\pi\Delta S}{\lambda}\left[\sin(\theta_1+\theta_0)+\sin(\theta_2+\theta_0)+\frac{x_s}{z_n}(\cos^2\theta_1+\cos^2\theta_2)+\sin(\theta_1+\theta_2)\cos(\theta_1-\theta_2)\right]\\&-\frac{2\pi\Delta S}{\lambda z_n}\sin(\theta_1+\theta_2)[x\sin(\theta_1-\theta_2)+(z-z_n)\cos(\theta_1-\theta_2)=\Delta\Phi(x,z).\end{aligned}\tag{7}$$

The phase is now a linear function of z and a nonlinear function of x. With this approximation the phase corresponding to only the object depth (z coordinate) can be easily obtained by experimentally or analytically correcting the raw measured phase.

2.1. *Experimental correction*

If we make a measurement of a plane which is normal to the view direction and is located at $z=z_n$, the phase of this measurement is

$$\Delta\Phi(z=z_n)=\frac{2\pi}{\lambda}C(\theta_1,\theta_2)-\frac{2\pi\Delta S}{\lambda z_n}x\sin(\theta_1+\theta_2)\sin(\theta_1-\theta_2),\tag{8}$$

where $C(\theta_1,\theta_2)$ represents the first term in equation (7). This phase information is saved as a calibration of the system. In the case of a symmetric and collimated illumination ($\theta_1=\theta_2$), $C(\theta_1+\theta_2)$ is a constant. The measurement data are homo-

geneous over the whole field. When the measured phase is $\Delta\Phi$ the corrected phase can be obtained through

$$\Delta\Phi_c = \Delta\Phi(z=z_n) - \Delta\Phi$$
$$= \frac{2\pi\Delta S}{\lambda z_n}(z-z_n)\sin(\theta_1+\theta_2)\cos(\theta_1-\theta_2). \tag{9}$$

2.2. *Analytical correction*

The phase can be analytically corrected if the measuring area (X, Y coordinates) and system parameters (i.e. x_s, z_n and ΔS) are already known. For example,

$$\Delta\Phi_c = \frac{2\pi}{\lambda}C(\theta_1,\theta_2) - \frac{2\pi\Delta S}{\lambda z_n}x\sin(\theta_1+\theta_2)\sin(\theta_1-\theta_2) - \Delta\Phi(x), \tag{10}$$

where θ_1, θ_2 and $C(\theta_1, \theta_2)$ are functions of x only, which can be well defined. After correction the depth of the object can be obtained through

$$h = z - z_n$$
$$= \frac{\lambda z_n \Delta\Phi_c}{2\pi\Delta S\sin(\theta_1+\theta_2)\cos(\theta_1-\theta_2)}, \tag{11a}$$

and the contour interval (the depth difference corresponding to a 2π phase difference) in the corrected data is then

$$d = \frac{\lambda z_n}{\Delta S\sin(\theta_1+\theta_2)\cos(\theta_1-\theta_2)}. \tag{11b}$$

For a symmetric and collimated illumination ($\theta_1=\theta_2=\theta_0, \Delta\theta_1=\Delta\theta_2=\Delta\theta_0=(\Delta S)\cos\theta_0/z_n$), we have (a constant is omitted):

$$\Delta\Phi_c = \Delta\Phi = \frac{2\pi}{\lambda}2(z-z_n)\Delta\theta_0\sin\theta_0, \tag{12}$$

and

$$h = z - z_n = \frac{\lambda\Delta\Phi}{4\pi\Delta\theta_0\sin\theta_0}, \tag{13a}$$

$$d = \frac{\lambda}{2\Delta\theta_0\sin\theta_0}, \tag{13b}$$

which are the same as described in [9].

3. Experimental results

The experimental arrangement is shown in figure 3. An 80 mW frequency-doubled Nd^+YAG laser ($\lambda = 0{\cdot}533\,\mu m$) was used as a coherent illumination source. The divergence of the laser beam was controlled by a lens. To produce correlation fringes the mirror before the beam splitter was shifted after the first exposure. In order to keep the source shift in the perpendicular direction to the principal ray, the lens was shifted along the optical axis to compensate for the axial shift introduced by shifting the mirror. The aperture was chosen so that the speckle size on the CCD chip was about one pixel size (in our case it was 11 μm) to obtain the best contrast for the correlation fringes. The images acquired by the CCD camera were processed by

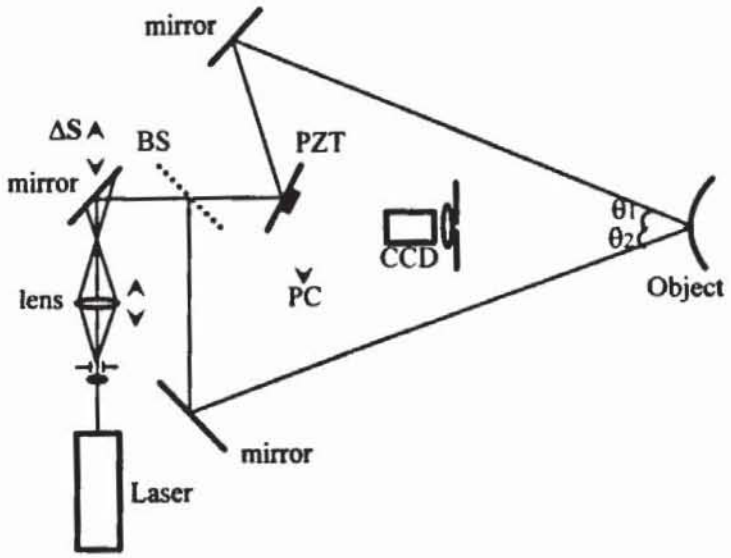

Figure 3. Set-up for ESPI contouring employing divergent beams.

a personal computer (PC) with a frame grabber board. To obtain a symmetric curvature difference on the object surface, the path lengths of two illumination beams should be the same, and the angle between the principal ray of each of the beams and the view direction should also be the same. In addition, both principal rays and their shifts should be in one plane. In this case, the sensitivity vector of the measurement or the contour plane is along the view direction and the fringe interpretation is simple. Referring to the theoretical analysis in the last section, the measured phase should be corrected to give true information about the object contour.

For an object field of 139 mm × 118 mm we chose $z_n = 1201{\cdot}6$ mm and $x_s = 614{\cdot}9$ mm to set the condition $z_n \gg \Delta S$ and $|\mathbf{r}|$ which allows measured data to be corrected experimentally or analytically. The system was calibrated by taking a set of measurements of a reference plane corresponding to different measurement sensitivities, i.e. different shifts of the beam, before formal measurements were made. The reference plane was normal to the viewing direction and located at the intersection between the principal rays of two beams. Under collimated illumination, the phase of the measurement is homogeneous over the whole field, but this is not the case for divergent illumination. The wrapped phase of the measurement of a reference plane with a beam shift of 100 μm ($\Delta S = 100$ μm) is shown in figure 4 with a 27·1° angle between the principal ray and the view direction ($\theta_0 = 27{\cdot}1°$). The phase was calculated with the phase-shifting method. The phase shifting in one illumination beam was introduced by a piezoelectric-transducer (PZT)-driven mirror. Because each ray in a divergent beam has a different reflection angle on the mirror, the mirror shift introduces different phase shifting for each ray. To eliminate this source of error, a Carré phase-shifting algorithm was used. This requires four phase-stepped measurements, i.e.,

$$\begin{aligned}
I_1(x,y) &= a(x,y) + b(x,y)\cos[\Delta\Phi(x,y) - 3\zeta(x,y)/2],\\
I_2(x,y) &= a(x,y) + b(x,y)\cos[\Delta\Phi(x,y) - \zeta(x,y)/2],\\
I_3(x,y) &= a(x,y) + b(x,y)\cos[\Delta\Phi(x,y) + \zeta(x,y)/2],\\
I_4(x,y) &= a(x,y) + b(x,y)\cos[\Delta\Phi(x,y) + 3\zeta(x,y)/2],
\end{aligned} \tag{14}$$

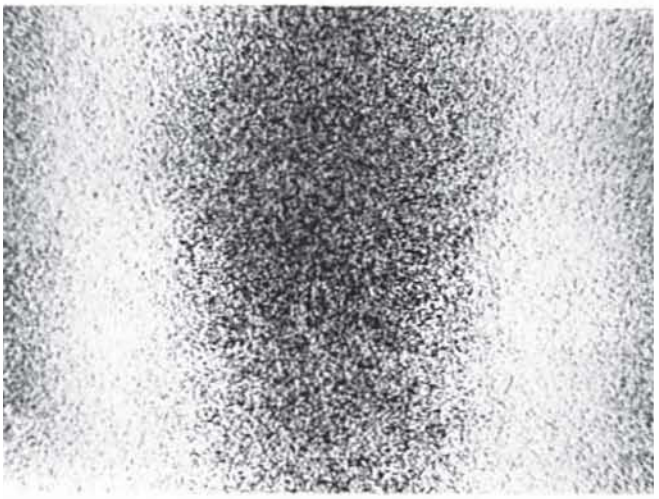

Figure 4. Raw phase of the measurement of a reference plane.

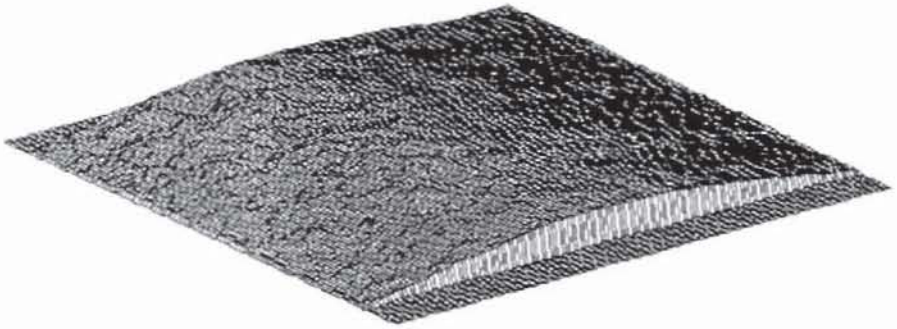

Figure 5. 3D plot of the measurement of the reference plane.

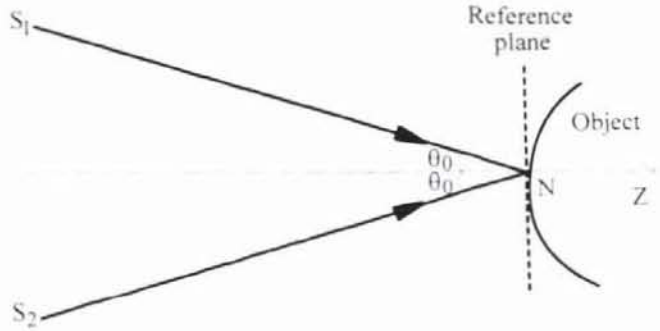

Figure 6. Location of the reference plane.

where $I_i(x, y)$ $(i = 1, 2, 3, 4)$ are the intensities of the four measurements at the image point (x, y), $a(x, y)$ is the mean intensity and $b(x, y)$ is the intensity modulation. $\Delta\Phi(x, y)$ is the phase to be measured, and $\zeta(x, y)$ is the phase shift. The phase can be obtained from these four equations as

$$\tan(\Delta\Phi) = \frac{\{[3(I_2 - I_3) - (I_1 - I_4)][(I_2 - I_3) + (I_1 - I_4)]\}^{1/2}}{(I_2 + I_3) - (I_1 + I_4)}. \tag{15}$$

To determine the phase modulo 2π, the signs of quantities proportional to $\sin(\Delta\Phi)$ and $\cos(\Delta\Phi)$ must be examined [12]. After an edge-preserving filtering and an integration of the 2π ambiguities, the phase data for the calibration were stored in the computer. The pseudo-three-dimensional (3D) plot is shown in figure 5. The test object then replaced the reference plane with its nearest point to the viewpoint just touching the reference plane (see figure 6). A tilted plane surface was chosen as a

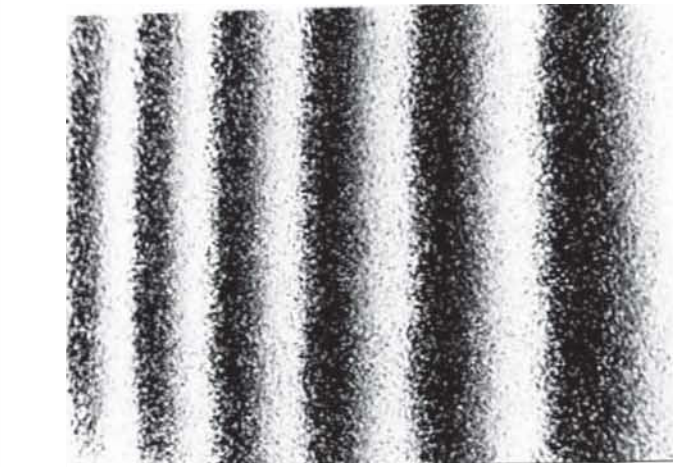

Figure 7. Raw phase of measurement on a wedge.

Figure 8. 3D plot of the measurement on a wedge.

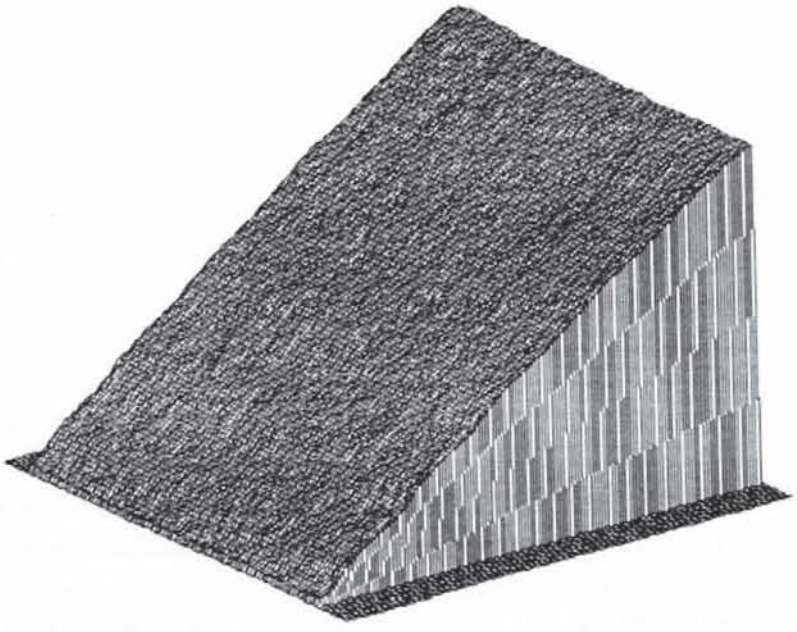

Figure 9. Experimentally compensated data from figure 8.

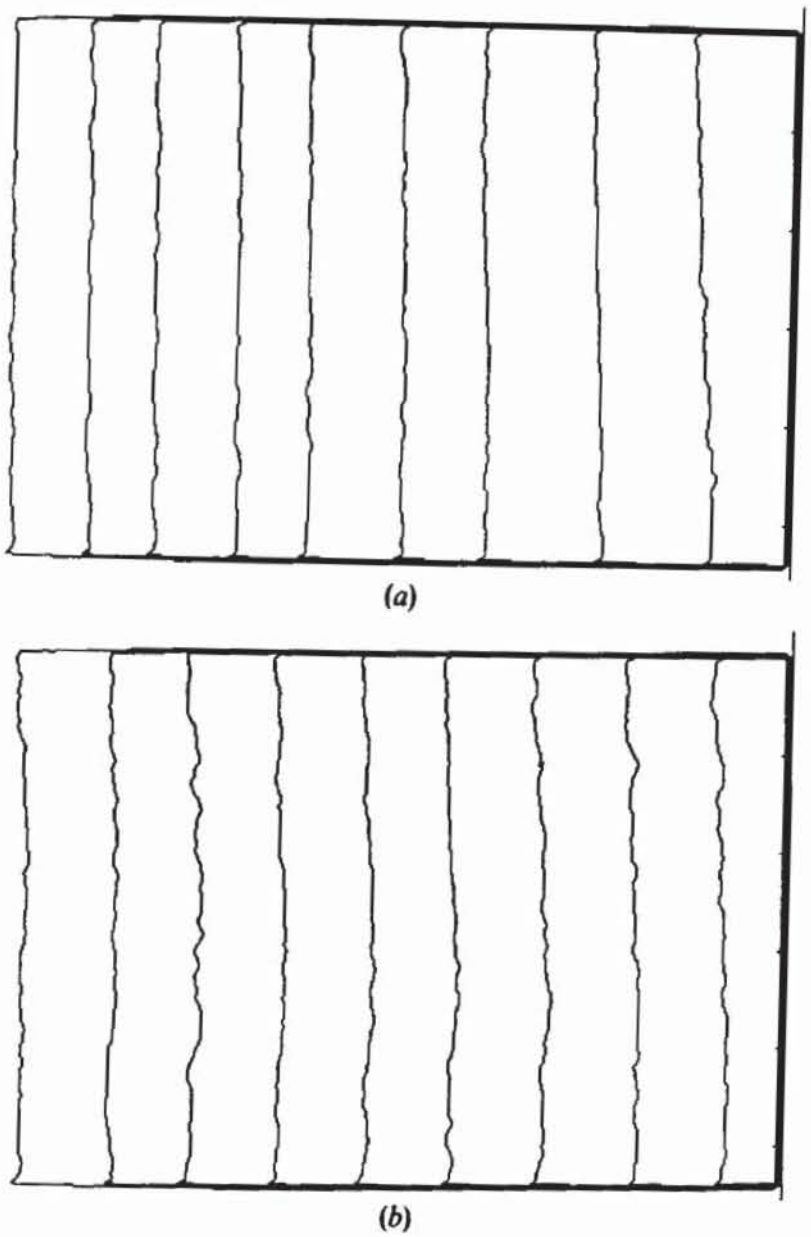

Figure 10. Contour maps of (*a*) the raw measurement and (*b*) its compensation.

simple object and the measured area was chosen to be the same as in the calibration. After making a measurement with the same sensitivity ($\Delta S = 100\,\mu m$), we obtained the raw phase map shown in figure 7. The fringes have different spacings from one part of the surface to another owing to the different curvatures of the wavefronts on the surface. The pseudo-3D plot is shown in figure 8. The surface is curved in this representation. A compensation can be made by simply subtracting the data from the previous stored data. This represents the departure of the object surface from the reference plane. The compensated data is graphically presented in figure 9. Contour maps of the raw measurement and its correction are given in figures 10 (*a*) and (*b*). The depth difference between two adjacent contour lines is 3·3 mm. The contour lines have non-equal spacing in the raw measurement but nearly equal spacing in the compensation. Unfortunately, the noise in the corrected data is slightly greater than that in the uncorrected data because it is a combination of the noise from two measurements. An analytical compensation for the measurement data was made with a computer program according to equation (10), in which the input experi-

Figure 11. Difference between the analytically compensated data and the simulated data.

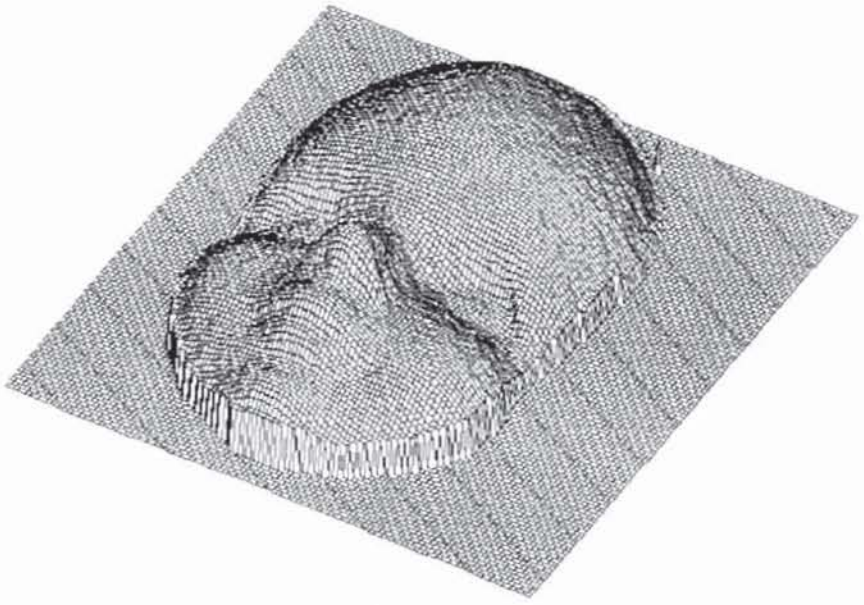

(*a*)

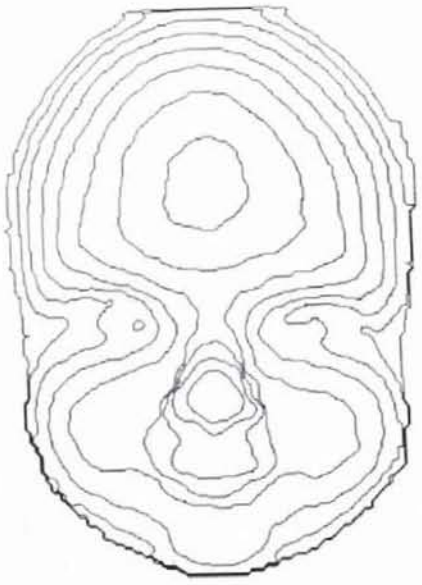

(*b*)

Figure 12. Experimental results on a complex object: (*a*) the 3D plot and (*b*) the contour map.

mental parameters were $\lambda = 0{\cdot}533\,\mu m$, $x_s = 614{\cdot}9\,mm$, $z_n = 1201{\cdot}6\,mm$, $\Delta S = 100\,\mu m$, and the maximum x coordinate and the maximum y coordinate of the measured area were 69·5 and 59 mm, respectively. The difference between the analytically corrected data and a simulated wedge data is graphically shown in figure 11. The slight waves in the graphics probably resulted from detection nonlinearities [12]. The root mean square (r.m.s.) value of this difference was about 0·21 mm. The r.m.s. value of the difference between the experimentally corrected data and the simulated data was about 0·46 mm. Taking the difference between equations (6) and (7) we obtain the maximum phase error, which was less than 5% in this experiment. This includes a 2% error from the first term and a 5% error from the second term in equation (5), where z_n was about 20 times greater than $|\mathbf{r}|$. When z_n is 10 times greater than $|\mathbf{r}|$, the phase error will be about 12%.

As an example, a face model was used as a complex object. The measurement area under divergent illumination was about 80 mm × 110 mm. The 3D representation and the contour map of the test surface were obtained by using the experimental method described above (see figures 12 (*a*) and (*b*)). The depth difference between two neighbouring contour lines was 3·0 mm.

4. Discussion and conclusion

The above analysis shows that the measured phase has a complicated dependence on the coordinates of a test object when divergent illumination is employed. To obtain exact contour information about the object a numerical solution should be taken. If some experimental conditions are satisfied, for example if the illumination geometry is much greater than the object dimensions and the source shift, which is true in most practical cases, the measured phase can be corrected analytically or experimentally. In the present work these corrections were made with two orders of approximation: (i) $z_n \gg \Delta S$, and (ii) $z_n \gg |\mathbf{r}|$. The first approximation is always true because z_n is at least 10^3 times greater than ΔS, but the second one should be considered carefully.

With these approximations the Y component in equation (6) disappears. This means that a divergent illumination has little effect on the measurement data in the Y direction, which is perpendicular to the plane on which the sources, their shifts and the viewpoint are located. Measurement of a plane tilted in the Y direction is shown in figure 13 (*a*). The line spacing is nearly fixed without correction. The slight curvature in the contour lines results from the influence of the X component in equation (7). It can be corrected by using the above methods. An analytically corrected result is shown in figure 13 (*b*).

A correction for divergent illumination needs to be considered when the difference of the wavefront curvatures on the object is significantly large. From our experiments this is the case when the data from the measurement of the reference plane are significantly larger than the noise contributions in the experimentally corrected data. Otherwise, equation (13) can be approximately applied to the case of divergent illumination.

In order to shift the illumination beams the lens can be shifted in a direction perpendicular to the optical axis (see figure 3), as in the case of collimated illumination [5]. However, the correlation between two speckle patterns before and after the wavefront change is reduced very fast when the shift is increased. This can be observed by viewing real-time subtraction fringes. However, the problem becomes much smaller when a mirror shift is employed instead of a lens shift.

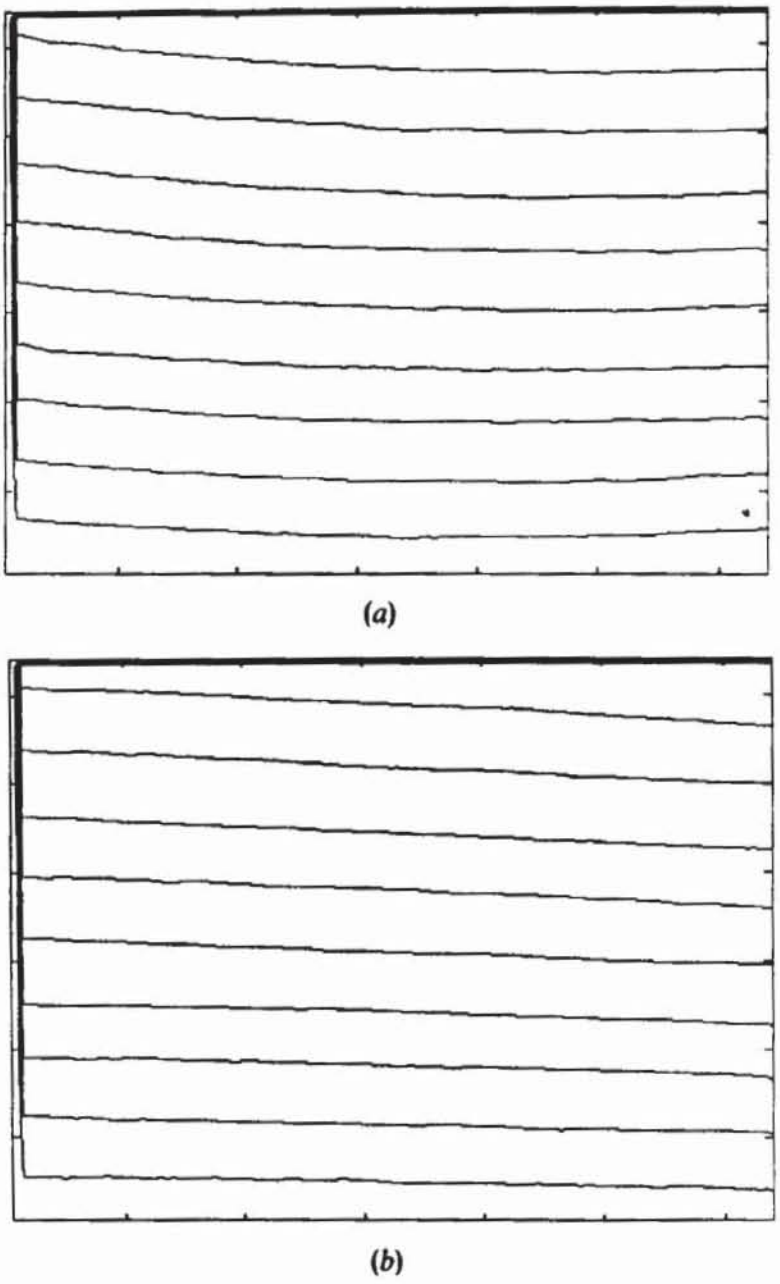

(*a*)

(*b*)

Figure 13. A contour map of a vertically tilted wedge (*a*) without and (*b*) with compensation.

Appendix A

Parameter $C(\alpha_1, \alpha_2, \theta_1, \theta_2)$

The parameter $C(\alpha_1, \alpha_2, \theta_1, \theta_2)$ was defined in section 2 as

$$C(\alpha_1, \alpha_2, \theta_1, \theta_2) = (\mathbf{I}'_{01} \cdot \mathbf{K}'_1 - \mathbf{I}'_{02} \cdot \mathbf{K}'_2 - \mathbf{I}_{01} \cdot \mathbf{K}_1 + \mathbf{I}_{02} \cdot \mathbf{K}_2). \tag{A 1}$$

Referring to figure A1 we have

$$\mathbf{K}_1 = (\cos\alpha_1 \sin\theta_1, \sin\alpha_1, \cos\alpha_1 \cos\theta_1), \tag{A 2 a}$$

$$\mathbf{K}_2 = [\cos\alpha_2 \sin(-\theta_2), \sin\alpha_2, \cos\alpha_2 \cos(-\theta_2)], \tag{A 2 b}$$

$$\mathbf{K}'_1 = (\cos\alpha'_1 \sin\theta'_1, \sin\alpha'_1, \cos\alpha'_1 \cos\theta'_1), \tag{A 2 c}$$

$$\mathbf{K}'_2 = [\cos\alpha'_2 \sin(-\theta'_2), \sin\alpha'_2, \cos\alpha'_2 \cos(-\theta'_2)], \tag{A 2 d}$$

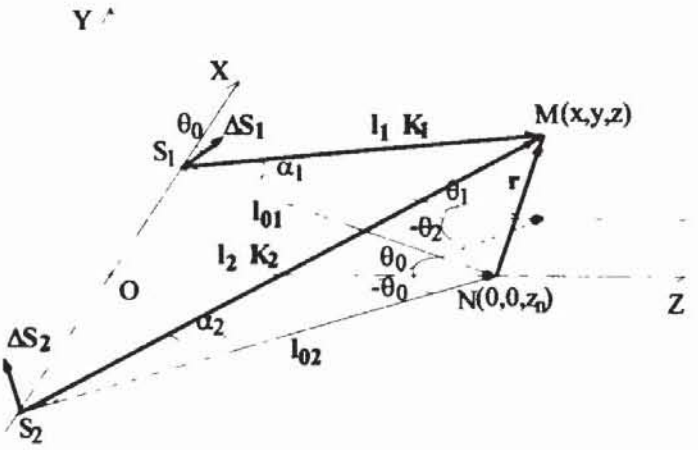

Figure A1. Vector geometry of dual-beam contouring.

where all angles are assumed to be positive, and

$$\Delta\mathbf{S}_1 = (\Delta S\cos\theta_0, 0, \Delta S\sin\theta_0), \tag{A 3 a}$$

$$\Delta\mathbf{S}_2 = [\Delta S\cos(-\theta_0), 0, \Delta S\sin(-\theta_0)], \tag{A 3 b}$$

and

$$\mathbf{l}_{01} = (-x_s, 0, z_n), \tag{A 4 a}$$

$$\mathbf{l}_{02} = (x_s, 0, z_n), \tag{A 4 b}$$

$$\mathbf{l}'_{01} = (-x_s - \Delta S\cos\theta_0, 0, z_n - \Delta S\sin\theta_0), \tag{A 4 c}$$

$$\mathbf{l}'_{02} = (x_s - \Delta S\cos\theta_0, 0, z_n + \Delta S\sin\theta_0), \tag{A 4 d}$$

and

$$\mathbf{l}_1 = (x - x_s, y, z), \tag{A 5 a}$$

$$\mathbf{l}_2 = (x + x_s, y, z), \tag{A 5 b}$$

$$\mathbf{l}'_1 = [(x - x_s) - \Delta S\cos\theta_0, y, z - \Delta S\sin\theta_0], \tag{A 5 c}$$

$$\mathbf{l}'_2 = [(x + x_s) - \Delta S\cos\theta_0, y, z + \Delta S\sin\theta_0]. \tag{A 5 d}$$

$\alpha_1, a_2, \alpha'_1, \alpha'_2, \theta_1, \theta_2, \theta'_1, \theta'_2$ and θ_0 can be represented as follows:

$$\tan\alpha_1 = \frac{y}{[(x-x_s)^2 + z^2]^{1/2}}, \tag{A 6 a}$$

$$\tan\alpha_2 = \frac{y}{[(x+x_s)^2 + z^2]^{1/2}}, \tag{A 6 b}$$

$$\tan\alpha'_1 = \frac{y}{[(x - x_s - \Delta S\cos\theta_0)^2 + (z - \Delta S\sin\theta_0)^2]^{1/2}}, \tag{A 6 c}$$

$$\tan\alpha'_2 = \frac{y}{[(x + x_s - \Delta S\cos\theta_0)^2 + (z + \Delta S\sin\theta_0)^2]^{1/2}}, \tag{A 6 d}$$

$$\tan\theta_1 = \frac{x_s - x}{z}, \tag{A 6 e}$$

$$\tan\theta_2 = \frac{x_s + x}{z}, \tag{A 6 f}$$

$$\tan\theta_1' = \frac{x_s - x + \Delta S\cos\theta_0}{z - \Delta S\sin\theta_0}, \tag{A 6g}$$

$$\tan\theta_2' = \frac{x_s + x - \Delta S\cos\theta_0}{z + \Delta S\sin\theta_0}, \tag{A 6h}$$

$$\tan\theta_0 = \frac{x_s}{z_n}. \tag{A 6i}$$

For $\Delta S \ll z, x_s$, we have

$$\begin{aligned}\cos\alpha_1' &= \frac{[(x - x_s - \Delta S\cos\theta_0)^2 + (z - \Delta S\sin\theta_0)^2]^{1/2}}{[(x - x_s - \Delta S\cos\theta_0)^2 + y^2 + (z - \Delta S\sin\theta_0)^2]^{1/2}},\\ &\cong \frac{[(x - x_s)^2 + z^2]^{1/2}}{[(x - x_s)^2 + y^2 + z^2]^{1/2}},\\ &= \cos\alpha_1,\end{aligned} \tag{A 7a}$$

$$\begin{aligned}\cos\alpha_2' &= \frac{[(x + x_s - \Delta S\cos\theta_0)^2 + (z + \Delta S\sin\theta_0)^2]^{1/2}}{[(x + x_s - \Delta S\cos\theta_0)^2 + y^2 + (z + \Delta S\sin\theta_0)^2]^{1/2}},\\ &\cong \frac{[(x + x_s)^2 + z^2]^{1/2}}{[(x + x_s)^2 + y^2 + z^2]^{1/2}},\\ &= \cos\alpha_2,\end{aligned} \tag{A 7b}$$

$$\begin{aligned}\sin(\theta_1' + \theta_0) &= \frac{(x_s - x)z_n + x_s z + \Delta S(z_n\cos\theta_0 - x_s\sin\theta_0)}{\{[(x_s - x + \Delta S\cos\theta_0)^2 + (z - \Delta S\sin\theta_0)^2](x_s^2 + z_n^2)\}^{1/2}},\\ &\cong \frac{(x_s - x)z_n + x_s z}{\{[(x_s - x)^2 + z^2](x_s^2 + z_n^2)\}^{1/2}},\\ &= \sin(\theta_1 + \theta_0),\end{aligned} \tag{A 7c}$$

and

$$\begin{aligned}\sin(\theta_2' + \theta_0) &= \frac{(x_s + x)z_n + x_s z - \Delta S(z_n\cos\theta_0 - x_s\sin\theta_0)}{\{[(x_s + x - \Delta S\cos\theta_0)^2 + (z + \Delta S\sin\theta_0)^2](x_s^2 + z_n^2)\}^{1/2}},\\ &\cong \frac{(x_s + x)z_n + x_s z}{\{[(x_s + x)^2 + z^2](x_s^2 + z_n^2)\}^{1/2}},\\ &= \sin(\theta_2 + \theta_0).\end{aligned} \tag{A 7d}$$

Therefore

$$\begin{aligned}C(\alpha_1, \alpha_2, \theta_1, \theta_2) \cong & -x_s(\Delta\theta_1\cos\alpha_1\cos\theta_1 + \Delta\theta_2\cos\alpha_2\cos\theta_2)\\ & - z_n(\Delta\theta_1\cos\alpha_1\sin\theta_1 + \Delta\theta_2\cos\alpha_2\sin\theta_2)\\ & - \Delta S[\cos\alpha_1\sin(\theta_1' + \theta_0) + \cos\alpha_2\sin(\theta_2' + \theta_0)]\\ \cong & -\Delta S\left\{\frac{x_s}{z}(\cos\alpha_1\cos^2\theta_1 + \cos\alpha_2\cos^2\theta_2)\right.\\ & + \frac{z_n}{2z}[\sin(2\theta_1)\cos\alpha_1 + \sin(2\theta_2)\cos\alpha_2]\\ & \left. + \cos\alpha_1\sin(\theta_1 + \theta_0) + \cos\alpha_2\sin(\theta_2 + \theta_0)\right\},\end{aligned} \tag{A 8}$$

where $\Delta\theta_1=\theta_1'-\theta_1\cong\Delta S\cos\theta_1/z$, $\Delta\theta_2=\theta_2-\theta_2'\cong\Delta S\cos\theta_2/z$, which have the same sign, $\theta_1'+\theta_1\cong 2\theta_1$ and $\theta_2'+\theta_2\cong 2\theta_2$. If $z_n\gg|\mathbf{r}|$, or in other words $z_n\gg|x|, |y|, |z-z_n|$, we could have $\cos\alpha_1\cong\cos\alpha_2\cong 1$, $\theta_1\cong\arctan[(x_s-x)/z_n]$ and $\theta_2\cong\arctan[(x_s+x)/z_n]$. Equation (A 8) approximates to

$$C(\theta_1,\theta_2)\cong-\Delta S\left[\frac{x_s}{z_n}(\cos^2\theta_1+\cos^2\theta_2)+\sin(\theta_1+\theta_2)\cos(\theta_1-\theta_2)\right.$$
$$\left.+\sin(\theta_1+\theta_0)+\sin(\theta_2+\theta_0)\right]. \tag{A 9}$$

When a symmetric and collimated illumination is employed, i.e., $\alpha_1=\alpha_2=0$, $\theta_1=\theta_2=\theta_0$ and $\Delta\theta_1=\Delta\theta_2=\Delta\theta_0$, $C(\alpha_1,\alpha_2,\theta_1,\theta_2)$ is a constant.

Appendix B

Amount of $\mathbf{r}\cdot(\Delta\mathbf{K}_1-\Delta\mathbf{K}_2)$

According to equation (A 2) we have

$$\Delta\mathbf{K}_1-\Delta\mathbf{K}_2=(\mathbf{K}_1'-\mathbf{K}_1)-(\mathbf{K}_2'-\mathbf{K}_2)$$
$$\cong(\Delta\theta_1\cos\alpha_1\cos\theta_1-\Delta\theta_2\cos\alpha_2\cos\theta_2,\Delta\alpha_1\cos\alpha_1-\Delta\alpha_2\cos\alpha_2,$$
$$-\Delta\theta_1\cos\alpha_1\sin\theta_1-\Delta\theta_2\cos\alpha_2\sin\theta_2), \tag{B 1}$$

where $\cos\alpha_1'\cong\cos\alpha_1$, $\cos\alpha_2'\cong\cos\alpha_2$, $\sin(\alpha_1'-\alpha_1)\cong\alpha_1'-\alpha_1=\Delta\alpha_1$, $\sin(\alpha_2'-\alpha_2)\cong\alpha_2'-\alpha_2=\Delta\alpha_2$, $(\alpha_1'+\alpha_1)/2\cong\alpha_1$, $(\alpha_2'+\alpha_2)/2\cong\alpha_2$, $\sin(\theta_1'-\theta_1)\cong\theta_1'-\theta_1=\Delta\theta_1$, $\sin(\theta_2'-\theta_2)\cong\theta_2'-\theta_2=\Delta\theta_2$, $(\theta_1'+\theta_1)/2\cong\theta_1$ and $(\theta_2'+\theta_2)/2\cong\theta_2$, were used according to the condition $\Delta S\ll z, x_s$. The second term in equation (5) is then obtained through

$$\mathbf{r}\cdot(\Delta\mathbf{K}_1-\Delta\mathbf{K}_2)\cong\Delta S\left\{\frac{x}{z}(\cos\alpha_1\cos^2\theta_1-\cos\alpha_2\cos^2\theta_2)\right.$$
$$+y\cos\theta_0\left(\frac{\sin\alpha_1\cos\alpha_1}{[(x-x_s)^2+z^2]^{1/2}}-\frac{\sin\alpha_2\cos\alpha_2}{[(x+x_s)^2+z^2]^{1/2}}\right)$$
$$\left.-\frac{z-z_n}{2z}[\cos\alpha_1\sin(2\theta_1)+\cos\alpha_2\sin(2\theta_2)]\right\}, \tag{B 2}$$

where $\mathbf{r}=(x,y,z-z_n)$, $\Delta\theta_1\cong\Delta S\cos\theta_1/z$, $\Delta\theta_2\cong\Delta S\cos\theta_2/z$, $\Delta\alpha_1\cong\Delta S\sin\alpha_1\cos\theta_0/[(x-x_s)^2+z^2]^{1/2}$ and $\Delta\alpha_2\cong\Delta S\sin\alpha_2\cos\theta_0/[(x+x_s)^2+z^2]^{1/2}$ were employed. If the condition $z_n\gg|\mathbf{r}|$ is satisfied, we get $\cos\alpha_1\cong\cos\alpha_2\cong 1$ and $\sin\alpha_1\cong\sin\alpha_2\cong 0$. Therefore

$$\mathbf{r}\cdot(\Delta\mathbf{K}_1-\Delta\mathbf{K}_2)\cong-\frac{\Delta S}{z_n}\sin(\theta_1+\theta_2)[x\sin(\theta_1-\theta_2)+(z-z_n)\cos(\theta_1-\theta_2)]. \tag{B 3}$$

When a symmetric and collimated illumination is employed, i.e., $\alpha_1=\alpha_2=0$, $\theta_1=\theta_2=\theta_0$ and $\Delta\theta_1=\Delta\theta_2=\Delta\theta_0$, a simple formula can be then obtained:

$$\mathbf{r}\cdot(\Delta\mathbf{K}_1-\Delta\mathbf{K}_2)=-2(z-z_n)\Delta\theta_0\sin\theta_0. \tag{B 4}$$

References

[1] SPOOREN, R., 1992, *Opt. Engng*, **31**, 1000.
[2] PEDRINI, G., PFISTER, B., and TIZIANI, H., 1993, *J. mod. Optics*, **40**, 89.
[3] JOENATHAN, C., PFISTER, B., and TIZIANI, H., 1991, *Appl. Optics*, **29**, 1905.
[4] BERGQUIST, B. D., and MONTGOMERY, P., 1985, *Proc. SPIE*, **599**, 189.
[5] PENG, X., DIAO, H., ZOU, Y., and TIZIANI, H., 1992, *Optik*, **90**, 61.
[6] WINTHER, S., and SLETTEMOEN, G., 1984, *Proc. SPIE*, **473**, 44.
[7] KERR, D., VERA, R. R., and SANTOYO, F. M., 1991, *Proc. SPIE*, **1554A**, 668.
[8] GANESAN, A. R., and SIROHI, R. S., 1988, *Proc. SPIE*, **954**, 327.
[9] ZHOU, Y., DIAO, H., PENG, X., and TIZIANI, H., 1992, *Appl. Optics*, **31**, 6616
[10] BUTTERS, J. N., JONES, R., and WYKES, C., 1978, *Speckle Metrology*, edited by R. K. Erf (New York: Academic), p. 111.
[11] JONES, R., and WYKES, C., 1983, *Holographic and Speckle Interferometry* (Cambridge University Press).
[12] CREATH, K., 1988, *Progress in Optics*, Vol. XXVI, edited by E. Wolf (New York: Elsevier), p. 366.